AIP | Journal of Applied Physics

Latent heat of vaporization of nanofluids: Measurements and molecular dynamics simulations

S. Tanvir, S. Jain, and L. Qiao

Citation: Journal of Applied Physics **118**, 014902 (2015); doi: 10.1063/1.4922967
View online: http://dx.doi.org/10.1063/1.4922967
View Table of Contents: http://scitation.aip.org/content/aip/journal/jap/118/1?ver=pdfcov
Published by the AIP Publishing

Latent heat of vaporization of nanofluids: Measurements and molecular dynamics simulations

S. Tanvir,[a] S. Jain,[a] and L. Qiao[b]
School of Aeronautics and Astronautics, Purdue University, West Lafayette, Indiana 47907, USA

(Received 28 January 2015; accepted 12 June 2015; published online 2 July 2015)

This paper reports measured and calculated (through molecular dynamics simulations) latent heat of vaporization (H_{fg}) for water and ethanol based nanofluids. The experimental results showed that the addition of 3 wt. % Ag and Fe nanoparticles in water results in a substantial reduction in H_{fg} (25% and 17%, respectively). On the contrary, 3 wt. % Al addition slightly increases H_{fg} (3%). Similar trends were observed for ethanol based nanofluids: 3 wt. % addition of Ag and Fe resulted in a reduction in H_{fg} by 19% and 13%, respectively, whereas 3 wt. % Al addition resulted in an increases in H_{fg} by 2%. Molecular dynamics simulations, which determine H_{fg} by calculating the total enthalpy change of a system before and after vaporization from a molecular level, showed that the strength of bonding between the nanoparticles and the fluid molecules is the governing factor in the variation of H_{fg} upon particle addition. It was found that the strength of Al/water bonds was much greater than Ag/water, resulting in a reduction in H_{fg} for the Ag/water nanofluids.
 [http://dx.doi.org/10.1063/1.4922967]

I. INTRODUCTION

Nanofluids are liquids with stable suspension of a small amount of nanometer-sized particles (1–100 nm) such as metals, oxides, carbides, or carbon nanotubes. Such fluids exhibit much higher thermal conductivity and diffusivity as compared to the base fluid, and thus can be used for more effective cooling or heating for various thermal and energy applications.[1–3] Of late there has been an enhanced interest in the combustion and propulsion community in developing high-performance nanofluid-type fuels. Suspending energetic or catalytic nanomaterials in traditional liquid fuels have the potential to enhance performance of propulsion systems,[4–11] e.g., higher energy release, shortened ignition delay, increased burning rate, increased ignition probability, and enhanced catalytic effect.

Latent heat of vaporization, H_{fg} (energy needed to vaporize a liquid), is an important property in many thermal applications.[12] However, there are very few studies that have examined H_{fg} of nanofluids. It is one of the critical parameters in determining the burning rate of liquid fuels.[13,14] Sabourin *et al.*,[8,15] McCown and Petersen,[16] and Tanvir and Qiao[17] recently have shown that a small amount of addition of energetic or catalytic nanoparticles in a liquid fuel significantly enhances the burning rate of the resulting fuel. This is a significant finding because higher burning rate indicates more efficient combustion and potentially smaller combustor. The mechanisms responsible for burning rate enhancement, however, are complex, which require investigations of the effect of radiation absorption by the nanoparticles, possible enhancement in surface area for evaporation due to particle wetting, variation of surface tension, and surface energy at higher temperatures, as well as changes in latent heat of vaporization, all as a result of particle addition.

To fully understand the effects of adding nanoparticles to the base liquid on the enhancement of burning rate, it is important to quantify the changes in H_{fg} upon particle addition. From the scarce literature available, we find contradictory results. While studying H_{fg} of Al_2O_3/water nanofluids, experimental analysis conducted by Ameen *et al.*[12] shows a ~20% enhancement of H_{fg} with 2 vol. % addition of Al_2O_3 nanoparticles. Molecular dynamics (MD) modeling results of a platinum/water nanofluid also show an enhancement of ~20% with a 2 vol. % addition of platinum nanoparticles (particle size ~0.6 nm). Zhu *et al.*,[18] however, found a ~16% reduction in H_{fg} with the addition of only 0.4 vol. % of Al_2O_3 and 0.5 vol. % SiO_2 nanoparticles in water. More recent experimental work by Lee *et al.*[19] observed an opposite trend for graphite/water and silver/water nanofluids. It was found that adding 0.1 vol. % of 30 nm graphite to deionized water results in a 36% increase in H_{fg}. On the contrary, once 0.1 vol. % silver was added to deionized water, H_{fg} reduces by 30%. The authors attribute this behavior to the ability of the nanoparticles to break and reform hydrogen bonds around the nanoparticles. Graphite was attributed to strengthen these hydrogen bonds which resulted in an increase in H_{fg}. Silver on the other hand is thought to weaken these bonds, resulting in a reduction in H_{fg}.

Motivated by these, an experiment was developed to measure H_{fg} of selected nanofluids. Water and ethanol were considered as the base fluid. Nanoparticles of various materials, sizes, and concentrations were considered as additives. The experiment was supplemented by molecular dynamics simulations, which calculate H_{fg} based on the total enthalpy of the system prior to and after vaporization from a molecular level. Results from both experiments and molecular dynamics simulations show that the change in H_{fg} upon nanoparticle additional is heavily dependent on the type of

[a]S. Tanvir and S. Jain contributed equally to this work.
[b]Author to whom correspondence should be addressed. Electronic mail: lqiao@purdue.edu. Tel.: (765)494-2040.

the particle used. For example, a 25% reduction in H_{fg} was observed when only 1 wt. % of Ag was added to water. An opposite trend was observed for Al addition in water. Molecular dynamics simulations reveal that the different trends in H_{fg} observed are a result of the strength of bonds formed between the particles and the water molecules.

II. EXPERIMENTAL METHODS

A. Nanofluid preparation

The nanofluids were prepared using physical and chemical (where required) dispersion methodologies as discussed in the earlier studies.[6,20] The appropriate amounts of particles were first vigorously stirred with the base liquid, followed by sonication of the colloidal mixture in an ultrasonic disrupter (QSonica Q500A) to minimize and delay particle agglomeration. The sonication was performed in an ice bath to maintain a constant temperature of the nanofluid. The sonicator generated a series of 2 s long pulses with 2 s spacing. The mixture was sonicated for about 8 min. Ethanol and water were used as base fluids. Particles of 80 nm Al, 35 nm Ag, 25–35 nm Al_2O_3, 80 nm SiO_2, and 25 nm Fe (all purchased from Nanostructured and Amorphous Materials, Inc.) were considered as additives. The amount of particles added was measured using an analytical scale (Torban AGZN 100) with an accuracy of 0.1 mg. Nanofluid samples prepared maintained excellent suspension quality without the presence of a surfactant for the duration of the experiment.

B. Measurement of latent heat of vaporization

Figure 1 shows the experiment setup to measure the latent heat of vaporization of selected nanofluids. It includes a thin-walled square quartz cuvette (12.5 mm × 12.5 mm × 45 mm) used to carry the nanofluid. An Omega 28-gage Ni-Cr wire, inserted into the nanofluid, was used as a heating element. For water and ethanol based nanofluids, a heat gun was also used to provide an isothermal boundary approximately at the boiling point of the fluid at the cuvette walls. An Omega K-type thermocouple was inserted into the nanofluid during the experiment to monitor its temperature. Measurements were taken after a stable temperature at the boiling point of the base fluid had been reached. A Torban AGZN 100 scale with an accuracy of 0.1 mg was used to monitor the mass of the samples. The mass of the vapor was determined by measuring the weight of the sample prior to and after the duration of the experiment. The duration of the experiment was set to 5 min for water and 3 min for ethanol to achieve a reasonable mass change of 500 mg. The results were normalized to account for the vaporization due to the heat gun, which means that the amount of fluid vaporized because of the heat gun at the operating temperature was measured separately and subtracted from the total mass vaporized in each test. This was to ensure that only boiling was considered.[19] All experiments were performed at atmospheric pressure.

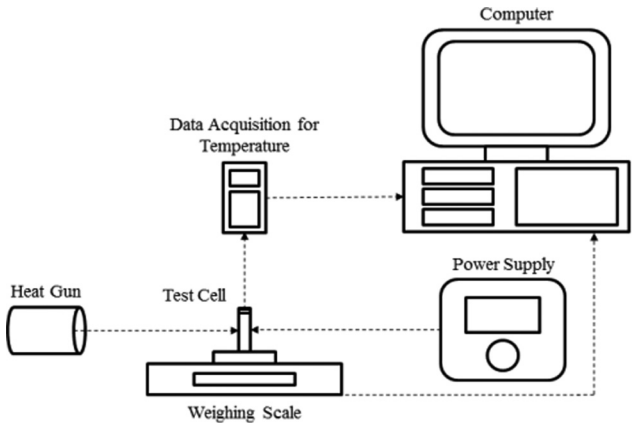

FIG. 1. Experimental setup to measure latent heat of vaporization.

Once the net mass $\dot{m}_{vapor}$ is obtained, H_{fg} can be calculated based on energy balance[21]

$$\dot{Q}_{in} - \dot{m}_{vapor} H_{fg} - \dot{Q}_{loss} = 0, \tag{1}$$

where Q_{in} is the rate at which heat is provided by the heating element and Q_{loss} is the heat loss during the vaporization process. Q_{in} was determined by dividing the square of the measured voltage across the wire by a known resistance at the operating temperature. Q_{loss} was negligible because the temperature difference between the cuvette surface and the nanofluid during the experiment was minimal. As such, Eq. (1) can be reduced to

$$H_{fg} = \frac{\dot{Q}_{in}}{\dot{m}_{vapor}}. \tag{2}$$

C. MD simulations

In addition to the experiments, MD simulations were performed to calculate the latent heat of vaporization of selected nanofluids. MD simulations, which use an intermolecular potential model to calculate the trajectory of all atoms in a system based on Newton's second law of motion, are typically limited to a small number of molecules because they are computationally expensive. As a result, we were not

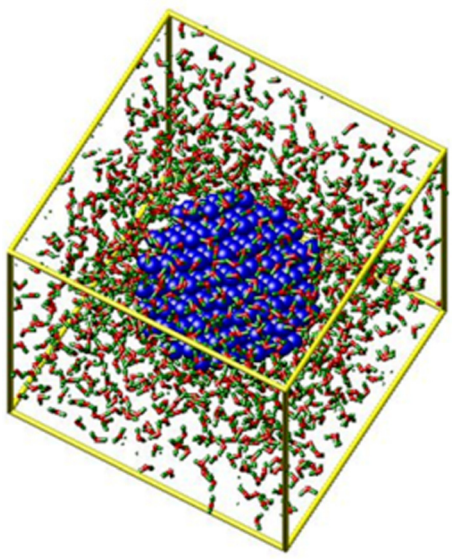

FIG. 2. Snapshot of an Ag nanoparticle (blue) surrounded by water (hydrogen atom: green; oxygen atom: red) in a simulation box.

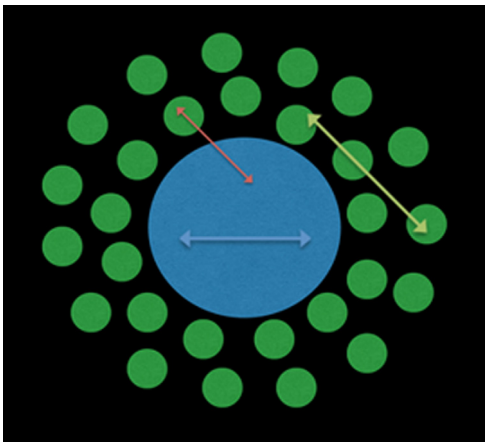

FIG. 3. Three types of interactions occurring in a nanofluid system. The green spheres represent water molecules. The red arrow represents interactions between the metal atoms and water molecules. The yellow arrow represents the interactions among water molecules. The blue arrow represents the interactions within the inner metal atoms of the nanoparticle.

allowed to consider particles having sizes that are comparable to those in the experiments. Rather, smaller particles were considered, and the goal was to understand the microscopic mechanisms responsible for the variation in H_{fg} upon addition of nanoparticles. Fundamentally, H_{fg} is the energy required for phase change from liquid to vapor at a constant temperature. This energy is used to overcome the molecular forces of attraction between the molecules of the liquid and bring them to vapor state where such attractions are minimal. MD simulations calculate the total intermolecular forces of all molecules in a system, including those between added nanoparticles and the base fluid, thus can help to explain why H_{fg} is enhanced or reduced because of addition of nanoparticles.

H_{fg} was obtained by calculating the difference in the enthalpy between the final vapor state and the initial liquid state. The two states were equilibrated separately at the same temperature and pressure. Because enthalpy is a thermodynamic state function, it is determined by the initial and final states only, regardless of the path from the initial state to the final state. Two nanofluid systems (Ag/water and Al/water) were simulated. They were chosen because the measured H_{fg} exhibit different trend—addition of Ag significantly reduces H_{fg} whereas addition of Al slightly increases H_{fg}. The simulations were performed considering various particle sizes (up to 15 nm) and mass fractions (up to 10%) to understand their effects on H_{fg}. Lastly, the computed H_{fg} for pure water was compared to the measured values that have been published in the literature. All the MD simulations were performed using the Large-scale Atomic/Molecular Massively Parallel Simulator Package (LAMMPS).[22] The details of the MD simulations, including the force fields and the computational method, are described in the following.

1. Description of the force fields

The simulation box contains one single nanoparticle surrounded by randomly distributed water molecules, as shown in Figure 2. The amount of water molecules in the simulation box (or the size of the simulation box) was determined by the weight percentage of the particles in water. Figure 3 shows three subsystems through which the intermolecular forces apply: solute-solvent, solvent-solvent, and solute-solute. Here, solvent refers to water molecules and solute refers to the metal atoms, which make up the nanoparticle.

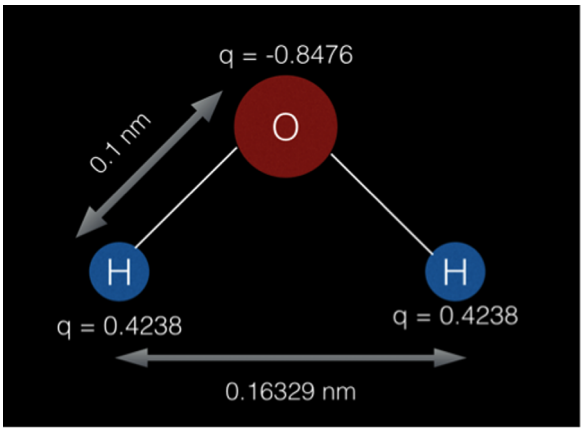

FIG. 4. Water SPC/E Model.[23]

a. Sub-system 1: H_2O–H_2O interactions (solvent-solvent interactions). The water molecules were modeled using the extended simple point charge (SPC/E) force field,[23] an improved version of the original SPC water model.[24] The SPC/E model considers water to be a rigid molecule with three point charges located at the oxygen and the two hydrogen atomic centers. In addition to the columbic interactions, the SPC/E model also considers dispersive Lennard-Jones (LJ) interactions between the oxygen atoms. The geometry of the model is illustrated schematically in Figure 4. The partial charges are $-0.8476|e|$ and $0.4238|e|$ for the oxygen and the hydrogen atom, respectively, where $|e|$ refers to the electron charge unit. A rigid tetrahedral angle (H–O–H) of 109.47° and a bond length (O-H) of 0.1 nm is assumed. The SHAKE algorithm was used to rigidify the water molecules. This was implemented by using the LAMMPS fix shake command.

The net pair potential acting between two water molecules can be expressed as follows:

$$E_{water} = E_{LJ} + E_{coul},$$

$$E_{LJ} = \begin{cases} 4\varepsilon_{OO}\left(\left(\frac{\sigma_{OO}}{R_{oo}}\right)^{12} - \left(\frac{\sigma_{OO}}{R_{oo}}\right)^{6}\right) & R_{oo} \le r_C, \\ 0 & R_{oo} > r_C, \end{cases} \tag{3}$$

$$E_{coul} = \sum_{i=1}^{3}\sum_{j=1}^{3}\frac{q_i q_j}{4\pi\epsilon_o r_{ij}}.$$

In Eq. (3), the L-J potential between the two oxygen atoms is represented by the term E_{LJ} with $\sigma_{OO} = 3.166$ Å and $\varepsilon_{OO} = 0.650$ kJ/mol, where R_{OO} is the distance between the two oxygen atoms and r_C is the cut-off distance beyond which the LJ potential is ignored. The electrostatic interactions are represented by the term E_{coul} that is the sum of nine

pairs of point charges, where ε_O is the vacuum permittivity, q_i and q_j are the point charges on the atoms belonging to different water molecules, and r_{ij} is the distance between the two sites.

b. Sub-system 2: Interactions between metal atoms (solute-solute interactions). The interactions among the metal atoms are not explicitly modeled but is implicitly taken into account through an external constrain force, which hold the metal atoms together as one rigid sphere. This was incorporated by applying a cluster potential as defined by the LAMMPS fix rigid style. Through this constrain, the coordinates and velocities of the atoms are updated such that the whole body moves as a single entity. However, LAMMPS require the pair-coefficients (force-fields) to be set between all the metal atoms before running the simulation, even though the interactions are not being used. For that purpose, the Embedded-atom Method (EAM) potential[25] was defined initially between the metal atoms but then was later excluded using the LAMMPS neigh modify exclude command.

c. Sub-system 3: Interactions between metal atoms and water molecules (solute-solvent interactions). The interactions between the metal atoms and water molecules are modeled using the L-J 6–12 potential as shown in Eq. (4)

$$E_{ij} = \begin{cases} 4\varepsilon_{ij}\left(\left(\frac{\sigma_{ij}}{R_{ij}}\right)^{12} - \left(\frac{\sigma_{ij}}{R_{ij}}\right)^{6}\right) & R_{ij} \le r_C, \\ 0 & R_{ij} > r_C, \end{cases} \quad (4)$$

where E_{ij} is the L-J potential between two atom types i and j. The values of σ_{ij} and ε_{ij} are obtained by using the Lorentz-Berthelot mixing rules[26,27]

$$\left(\sigma_{ij} = \frac{1}{2}(\sigma_i + \sigma_j)\right) \quad \text{and} \quad \left(\varepsilon_{ij} = \sqrt{\varepsilon_i \varepsilon_j}\right). \quad (5)$$

The LJ parameters for each atom type are given in Table I.

2. Molecular dynamics simulation parameters, convergence, and validation

The design of the MD simulation was limited by the available computational power (simulation time). Since, the total number of interactions in a system increases as N^2, which is very computationally expensive; a special mesh based technique (PPPM) is required to compute the long-range coulomb interactions. Since, the LJ potential decays as $1/r^6$, it is acceptable to use the cut-off and neglect the long-range LJ interactions. But, for the columbic forces, the potential decays as 1/r and the long-range coulomb interactions need to be considered. At distances $r < r_C$, the columbic interactions are computed directly, but for distances greater than r_C, the interactions are computed in the reciprocal space using the LAMMPS K-space command along with its PPPM (particle-particle particle-mesh solver, the computational cost is NlogN as compared to N^2) option.[30] A cut-off value of 1 nm was used (which is around 2.5 times the diameter of the atoms simulated).

TABLE I. Lennard-Jones parameters.[23,28,29]

Parameter	Oxygen (water)	Ag	Al
Σ	3.166 Å	2.644 Å	2.62 Å
E	0.650 kJ/mol	33.287 kJ/mol	37.839 kJ/mol

The NPT ensemble (constant number of particles (N), temperature (T), and pressure (P)) using the Nose-Hoover temperature thermostat[31] and the Nose-Hoover pressure barostat[32] was used to run the simulations. The rigid nanoparticles were simulated using the NVT fix rigid command. In addition, periodic boundary conditions were used in order to model the equilibrium physics of a realistic nanofluid system, which considers the nanoparticle-nanoparticle interactions through the presence of periodic images of the nanoparticle. The simulations were carried out using the leapfrog algorithm. A time-step sensitivity analysis was performed to ensure that the numerical results are independent of the timestep. Four timesteps (1, 2, 5, and 7 fs) were chosen to investigate the effect of the timestep on the results as shown in Figure 5. The particular case shown here is the Ag/water nanofluid system with 2 nm particle size and 3% by weight. The graph shows that the change in the enthalpy is very steep from 7 fs to around 2 fs and then it starts to flatten out. The change in H_{fg} between 1 fs and 2 fs is only 0.2%. As a result, 2 fs was chosen for all the simulations, since it ensures that the results obtained would be independent of the step size, with the least amount of computational time required. The relaxation time for the Nose-Hoover thermostat and the barostat was set to 0.2 ps and 2 ps, respectively, for the 2 fs case. For the other cases, the recommended relaxation time of 100 and 1000 timesteps for thermostat and barostat, respectively, was used.

The MD simulations were run in parallel using the MPI library installed on the Purdue research clusters, with each simulation using 7 nodes (and each node consist of 16 processors). The main technical challenge that was faced was to be able to equilibrate the system in the lowest possible simulation time. The total simulation time was restricted to 70 000 timesteps, which corresponds to 0.14 ns (using 2 fs

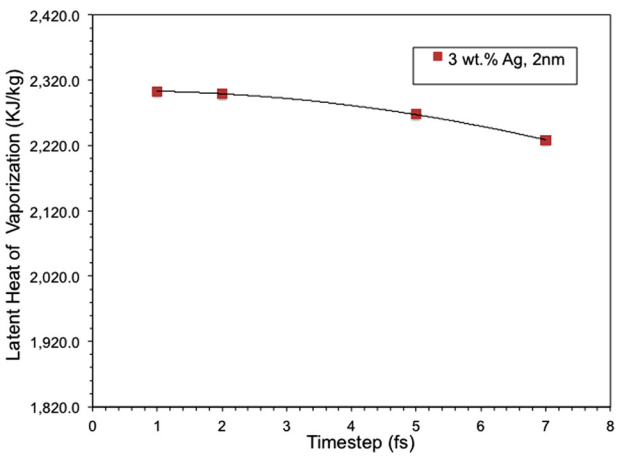

FIG. 5. Latent heat of vaporization as a function of the timestep for case 3, corresponding to 3 wt. % Ag-water nanofluid system with 2 nm particle size.

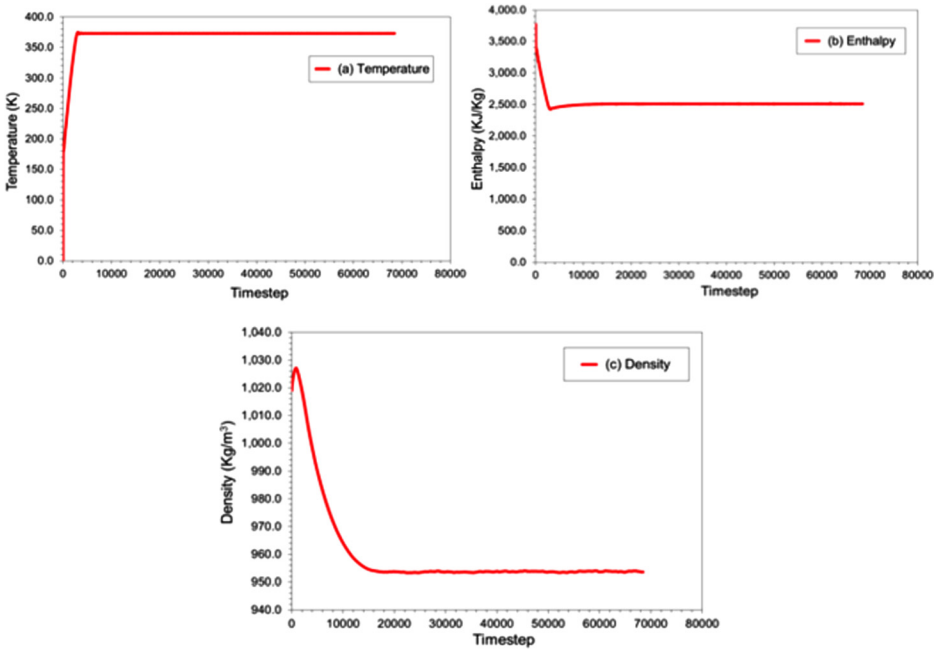

FIG. 6. Convergence plots for the (a) temperature, (b) enthalpy, and (c) density for the Al/water nanofluid system with 15 nm nanoparticle and 3% by weight.

timestep). This timestep was decided based on the convergence would be required for the 15 nm-sized nanoparticle systems to give accurate H_{fg} values and radial distribution function (RDF) plots. Moreover, the self-diffusion coefficient of pure water for the desired thermodynamic conditions, 373 K and 1 atm, came out to be 8.9×10^{-9} m^2/s. This value is similar to the experimental value of 8.6239×10^{-9} m^2/s obtained by Holz *et al.*[33] Using this self-diffusion coefficient value, the root mean square displacement of water molecules came out to be 2.73 nm for 70 000 time-steps or 0.14 ns. However, if the ballistic motion of the water molecules is considered then during these 70 000 time-steps, the water molecules would be able to move 82 nm (using 585 m/s, the thermal velocity of water), which is bigger than half of the largest box size that was simulated (120/2 = 60 nm). Figure 6 shows that the large-sized nanoparticle system (corresponding to 15 nm Al/water, 3% by weight) is well equilibrated within 70 000 time-steps.

Moreover, we also calculated the real time it took for the simulations to run. With the help of LAMMPS, we can output the loop time required to run the 70 000 timesteps. Table II shows the computational cost as a function of the number of water molecules simulated and the type of nanoparticle added. The most expensive simulation was the Ag/water, 15 nm, 1% by weight for which the computational cost was around 620 h (real time). Thus, the main challenge was the huge computational cost, which was addressed by choosing the maximum possible step size (2 fs) and the minimum number of timesteps that would give us accurate results. Table III summarizes all the systems that were simulated. Based on the desired weight percentage of the nanoparticle, the size of the nanoparticle was determined and then added to the system. Water molecules overlapping the added nanoparticle were deleted. As stated above, the enthalpy of vaporization of the desired system was obtained by subtracting the total enthalpy (total energy + Pressure × Volume) of the initial liquid system from the total enthalpy of water vapor (final state). The calculated H_{fg} of pure water came out to be 2354.81 kJ/kg, which is within the error bar of the experimentally obtained value of 2283.57 ± 91.54 kJ/kg in the literature. The calculated density of pure water is 932 kg/m^3, which is within 2.7% of the known theoretical value of 958 kg/m^3.

TABLE II. Simulations results: Computational cost.

System	wt. %	Number of water molecules simulated	Computational cost: Real time (h)	Nanoparticle size (nm)
Ag/Water	1	58 868 305	620	15
Ag/Water	3	18 162 741	180	15
Ag/Water	1	187 168	2.00	2
Ag/Water	3	40 221	0.7	2
Al/Water	1	15 884 305	240	15
Al/Water	3	4 974 741	80	15
Al/Water	1	40 221	1.00	2
Al/Water	3	11 710	0.5	2

III. RESULTS AND DISCUSSION

Figures 7 and 8 show the measured H_{fg} for water and ethanol based nanofluids, respectively. The measured H_{fg} for pure water (2283.57 ± 91.54 kJ/kg) and ethanol (891.97 ± 15.15 kJ/kg) are comparable to their known values of 2257 kJ/kg and 896 kJ/kg. This provides a validation of the present experimental method. Figure 7 shows that the addition of 3 wt. % Ag and Fe nanoparticles results is a substantial reduction in H_{fg} (25% and 17%, respectively). Also seen from Figure 7 is that the reduction of H_{fg} with the addition of 1 wt. % Ag is consistent with the findings of Lee *et al.*,[19] who measured H_{fg} using a similar method. The slight difference of H_{fg} between the present measurement and that by Lee *et al.* is attributed to the different particle sizes used in the experiment (35 nm vs. 20 nm). Furthermore, a somewhat opposite trend is observed for Al where a 3 wt. % addition leads to a 3% gain in latent heat of vaporization. In addition to metallic nanoparticles of Ag, Fe, and Al, catalytic nanoparticles such as Al_2O_3 and SiO_2 were also considered. Both

TABLE III. MD simulation matrix.

Case No.	System	wt. %	No. of water molecules	No. of metal atoms	Size (nm)
1	Pure water	0	40 500	0	…
2	Ag/water	1	187 168	240	2
3	Ag/water	3	40 221	240	2
4	Ag/water	1	58 868 305	103 308	15
5	Ag/water	3	18 162 741	103 308	15
6	Ag/water	10	4974 741	103 308	15
7	Al/water	1	40 221	264	2
8	Al/water	3	11 710	264	2
9	Al/water	1	15 884 305	111 589	15
10	Al/water	3	4974 741	111 589	15

resulted in a reduction in H_{fg} of water. A similar observation is made for ethanol based nanofluids where 3 wt. % addition of Ag and Fe resulted in a reduction in H_{fg} of the resulting nanofluid by 19% and 13%, respectively, whereas the addition of 3 wt. % Al in ethanol gave a rise in H_{fg} of 2%.

These results show that the type of the nanoparticles and the weight percentage have dominant effects on H_{fg} whereas the type of base fluid has little impact on how nanoparticles affect H_{fg} (increases or decrease). From a microscopic perspective, when nanoparticles are added to water, they may break the already existing hydrogen bonds between water molecules, and new bonds are formed between water molecules and the nanoparticles.[19] The strength of bonding between the nanoparticles and the base fluid will consequently affect H_{fg} of the nanofluid. The stronger these bonds, it will require more energy to vaporize the nanofluid, therefore increasing H_{fg}. It is therefore hypothesized that bonds formed between Ag-water/ethanol or Fe-water/ethanol are weaker than the bonds formed between Al-water/ethanol causing a significant reduction in H_{fg} for Ag and Fe nanofluids. This hypothesis is confirmed by the results obtained through MD simulations, which are discussed in the following.

Figure 9 shows the calculated H_{fg} for water-based nanofluids, considering 15 nm Ag and Al particles at varying concentrations. H_{fg} decreases upon Ag particle addition and increases with increasing Al nanoparticle addition. This opposite trend is consistent with what was observed in the

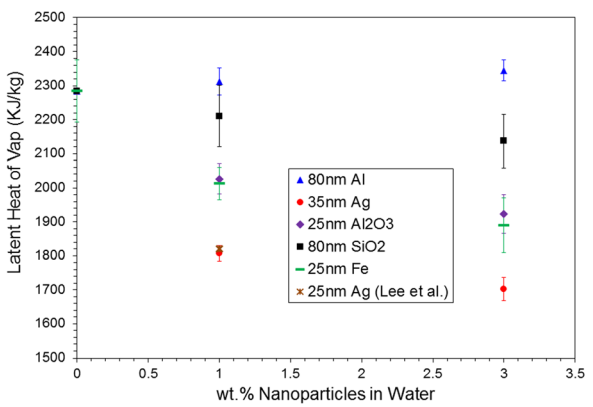

FIG. 7. Measured latent heat of vaporization of water based nanofluids.

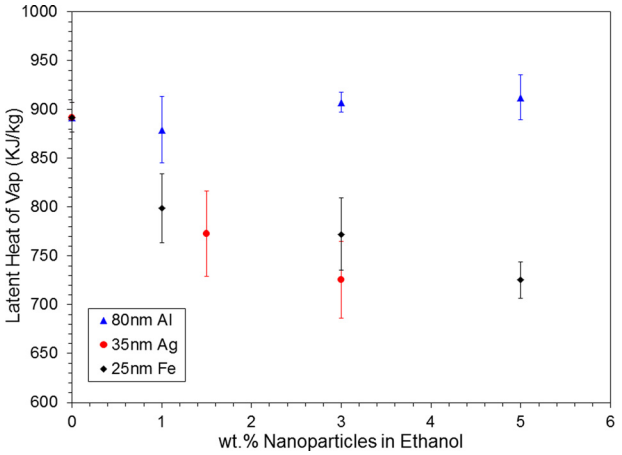

FIG. 8. Measured latent heat of vaporization of ethanol based nanofluids.

experiment as shown in Figure 7. Note the values of H_{fg} obtained from the MD simulations do not agree quantitatively with the measured values because smaller nanoparticles were simulated as a result of limited computing resources.

To understand the effect of particle addition on the structural arrangement of water molecules, RDFs were plotted for Ag/water and Al/water nanofluid systems, as shown in Figure 10. Figure 10(a) corresponds to 15 nm Al and Ag nanoparticles at 3 wt. %, while Figure 10(b) corresponds to 2 nm Al and Ag nanoparticles also at 3 wt. %. RDFs give the probability of finding an atom (molecule) at a distance r from another atom (molecule) and thus can describe the structure of a system. In Figure 10, RDFs are plotted between the metal atoms on the surface of the nanoparticle and the oxygen atom in water molecules. As such, r is the distance from the surface of the nanoparticle. In Figures 10(a) and 10(b), the first peak in the distributions is located at 2.89 Å and 2.91 Å for Al and Ag, respectively, corresponding to the average van der Waals radius of oxygen and the metal atom. These peaks indicate short-range order with water molecules being arranged in a definite pattern around the nanoparticle. This is a result of the attractive nature of the interactions at such distances. Moreover, the radial distribution approaches 1 as r tends to infinity, implying a complete long-range disorder. This is because at such large distances there are no interactions between nanoparticles and water molecules. For very short distances, the RDF(r) = 0 because of the strong repulsive forces between various atoms. The peak for the Al and Ag system occurs at the nearly same distance because their L-J parameter, σ, is almost identical, as shown in Table I. However, the magnitude of the peaks differs for the two systems. This is hypothesized to be one of the main reasons for the reduction in H_{fg} for Ag/water and increase in H_{fg} for Al/water. The magnitude of the peak gives the probability of finding an oxygen atom at a distance r. Therefore, for Al/water, we have a greater number of water molecules arranged around the nanoparticle. This can be explained from looking at the ε values of the L-J potential from Table I. Since, $\varepsilon_{AL} > \varepsilon_{Ag}$, the strength of Al-O interaction is much greater than Ag-O interaction; hence, more water molecules are attracted towards

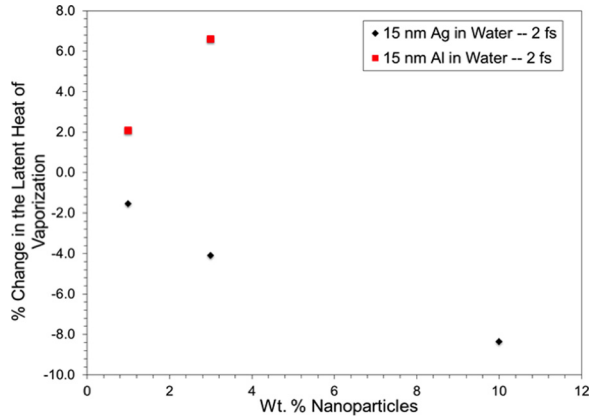

FIG. 9. Calculated latent heat of vaporization by MD simulations for water based nanofluids.

the Al surface atoms. Additionally, because the density of Ag atoms is four times of the density of Al atoms, there are four times as many water molecules in former system as compared to the latter, for the same nanoparticle size and weight percentage. Thus, the effect of the Al-O interactions has a more pronounced effect on the total energy of the system as compared to the Ag-O interactions resulting in a higher H_{fg} for the Al/water system. These results confirm the hypothesis that bonds formed between Ag-water are indeed weaker than those formed between Al-water resulting in opposite trends in H_{fg} upon nanoparticles addition for the two systems.

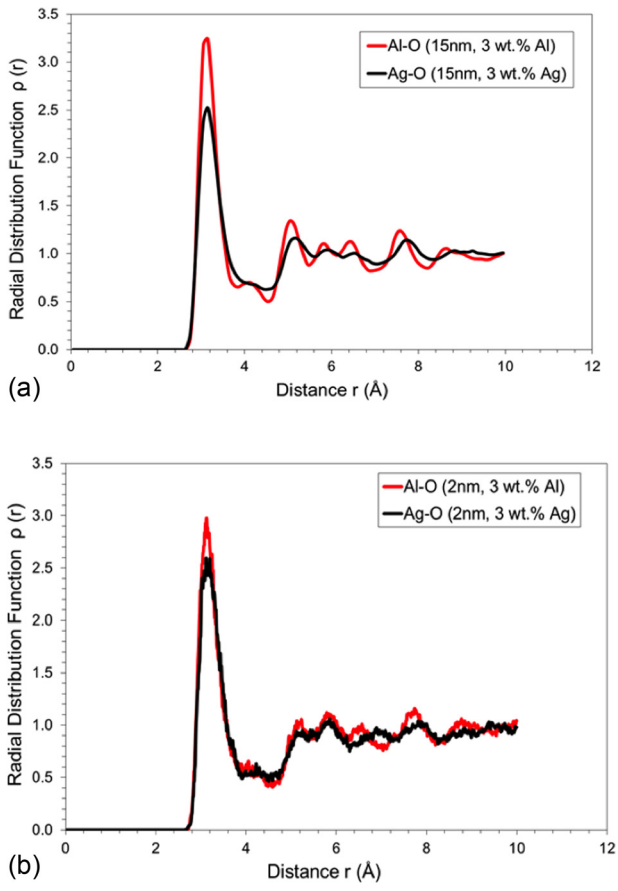

FIG. 10. Radial distribution function for Ag/water and Al/water systems for 15 nm (a) and 2 nm (b) nanoparticles.

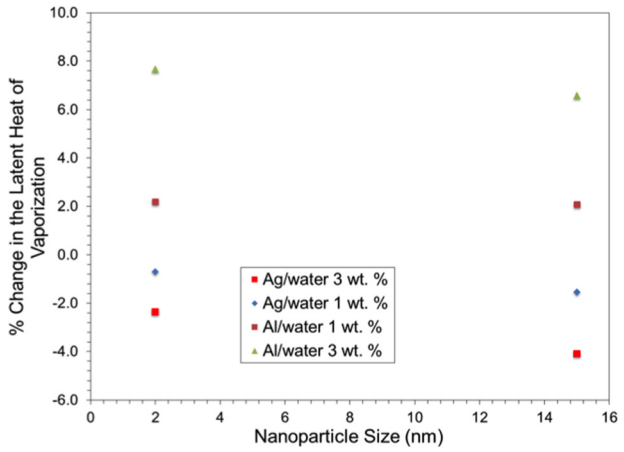

FIG. 11. Calculated latent heat of vaporization for Ag/water and Al/water at various particle sizes.

As mentioned earlier, limited computing power did not allow us to consider large nanoparticles as those used in the experiments. As a result, it is important to understand the effect of particle size on H_{fg}. Figure 11 shows the calculated H_{fg} for Al/water and Ag/water at two particles sizes. As the particle size is increased from 2 nm to 15 nm, H_{fg} for both the systems decreases. This is because the ratio of the number of interactions between the metals atoms and the water molecules to the number of the hydrogen bonds being broken decreases, as the particle size is increased for the same weight percentage. The number of interactions between the metals atoms and the water molecules decreases because with the increase in particles size, the percentage of the core metals atoms shielded from the outer surface atoms increases. As a result, the discrepancies between simulations and experiments would be reduced if real particle sizes as used in the experiment (~35 nm for Ag and ~80 nm Al) were considered in the MD simulations.

III. CONCLUSIONS

An experiment was developed to measure H_{fg} of selected nanofluids. Additionally, MD simulations were performed to calculate H_{fg} by considering three types of interactions in the system. Both measurements and simulations showed that a small amount of nanoparticle addition can significantly alter H_{fg} of the base fluid. The base fluid, however, had little impact on how particle addition changes H_{fg}. The experimental results showed that the addition of 3 wt. % Ag and Fe nanoparticles in water results is a substantial reduction in H_{fg} (25% and 17%, respectively). On the contrary, 3 wt. % Al addition slightly increases H_{fg} (3%). For ethanol based nanofluids, 3 wt. % addition of Ag and Fe resulted in a reduction in H_{fg} of the resulting nanofluid by 19% and 13%, respectively, and a similar amount of Al addition resulted in an increases in H_{fg} by 2%. MD simulations helped to determine that the strength of bonding between particles and the fluid molecules is the governing factor in the variation of H_{fg} upon particle addition. The strength of Al/water bonds was

much greater than Ag/water, resulting in a lower H_{fg} for the Ag/water nanofluid. Moreover, the particle size effect was also determined using the MD simulations. The H_{fg} for both the systems (Ag/water and Al/water) decreases with an increase in the nanoparticle size.

ACKNOWLEDGMENTS

This work has been supported by American Chemical Society Petroleum Research Fund.

[1]S. K. Das, S. U. S. Choi, and H. E. Patel, Heat Transfer Eng. **27**(10), 3–19 (2006).
[2]G. Ramesh and N. K. Prabhu, Nanoscale Res. Lett. **6**, 334 (2011).
[3]V. Sridhara and L. N. Satapathy, Nanoscale Res. Lett. **6**, 646 (2011).
[4]M. Jones, C. H. Li, A. Afjeh, and G. P. Peterson, Nanoscale Res. Lett. **6**, 246 (2011).
[5]C. Allen, G. Mittal, C. J. Sung, E. Toulson, and T. Lee, Proc. Combust. Inst. **33**, 3367–3374 (2011).
[6]Y. A. Gan and L. Qiao, Combust. Flame **158**(2), 354–368 (2011).
[7]Y. A. Gan and L. Qiao, Int. J. Heat and Mass Transfer **54**(23–24), 4913–4922 (2011).
[8]J. L. Sabourin, R. A. Yetter, B. W. Asay, J. M. Lloyd, V. E. Sanders, G. A. Risha, and S. F. Son, Propellants, Explos., Pyrotechn. **34**(5), 385–393 (2009).
[9]H. Tyagi, P. E. Phelan, R. Prasher, R. Peck, T. Lee, J. R. Pacheco, and P. Arentzen, Nano Lett. **8**(5), 1410–1416 (2008).
[10]B. Van Devener and S. L. Anderson, Energy Fuels **20**(5), 1886–1894 (2006).
[11]B. Van Devener, J. P. L. Perez, J. Jankovich, and S. L. Anderson, Energy Fuels **23**, 6111–6120 (2009).
[12]M. M. Ameen, K. Prabhul, G. Sivakumar, P. P. Abraham, U. B. Jayadeep, and C. B. Sobhan, Int. J. Thermophys. **31**(6), 1131–1144 (2010).
[13]R. H. Chen, T. X. Phuoc, and D. Martello, Int. J. Heat Mass Transfer **53**(19–20), 3677–3682 (2010).
[14]C. K. Law, Prog. Energy Combust. Sci. **8**(3), 171–201 (1982).
[15]J. L. Sabourin, R. A. Yetter, and V. S. Parimi, J. Propul. Power **26**(5), 1006–1015 (2010).
[16]K. W. McCown and E. L. Petersen, Combust. Flame **161**(7), 1935–1943 (2014).
[17]S. Tanvir and L. Qiao, J. Propul. Power **31**(1), 1–8 (2014).
[18]B. J. Zhu, W. L. Zhao, J. K. Li, Y. X. Guan, and D. D. Li, Mater. Sci. Forum **688**, 266–271 (2011).
[19]S. Lee, P. E. Phelan, L. Dai, R. Prasher, A. Gunawan, and R. A. Taylor, Appl. Phys. Lett. **104**(15), 151908 (2014).
[20]Y. A. Gan, Y. S. Lim, and L. Qiao, Combust. Flame **159**(4), 1732–1740 (2012).
[21]F. P. Incropera, *Fundamentals of Heat and Mass Transfer*, 6th ed. (John Wiley, Hoboken, NJ, 2007).
[22]S. Plimpton, P. Crozier, and A. Thompson, "LAMMPS-large-scale atomic/molecular massively parallel simulator," Sandia National Laboratories, Vol. 18 (2007).
[23]H. J. C. Berendsen, J. R. Grigera, and T. P. Straatsma, J. Phys. Chem. **91**(24), 6269–6271 (1987).
[24]H. J. C. Berendsen, J. P. M. Postma, J. P. M. van Gunsteren, and J. Hermans, paper presented at the Jerusalem Symposia on Quantum Chemistry and Biochemistry, Jerusalem, Israel, 13–16 April 1981.
[25]M. S. Daw and M. I. Baskes, Phys. Rev. Lett. **50**(17), 1285–1288 (1983).
[26]D. Berthelot, Compt. Rendus **126**, 1703–1855 (1898).
[27]H. A. Lorentz, Ann. Phys. **248**(1), 127–136 (1881).
[28]P. Guan, D. R. Mckenzie, and B. A. Pailthorpe, J. Phys.: Condens. Matter **8**(45), 8753–8762 (1996).
[29]P. Puri and V. Yang, J. Phys. Chem. C **111**(32), 11776–11783 (2007).
[30]O. Buneman, SIAM Rev. **25**(3), 425–426 (1983).
[31]S. Maruyama, *Molecular Dynamics Method for Microscale Heat Transfer* (Taylor and Francis, New York, 2000).
[32]S. Melchionna, G. Ciccotti, and B. L. Holian, Mol. Phys. **78**(3), 533–544 (1993).
[33]M. Holz, S. R. Heil, and A. Sacco, Phys. Chem. Chem. Phys. **2**(20), 4740–4742 (2000).